**Proceedings of the ASME 2020 International Design Engineering Technical Conferences &
Computers and Information in Engineering Conference
IDETC/CIE 2020
August 16-19, 2020, St. Louis, USA**

IDETC2020-22257

DESIGNING EXCITATION MANEUVERS WITH MAXIMAL PARAMETER SENSITIVITY FOR AN X-BY-WIRE AUTONOMOUS TRICYCLE

Yi-Ping Chen, Kuei-Yuan Chan*
Department of Mechanical Engineering
National Taiwan University
Taipei, Taiwan 10617
Email: {chenyp, chanky}@solab.me.ntu.edu.tw

ABSTRACT

Validation in vehicle engineering identifies and quantifies the differences between simulation models and experiment data. In this work we consider these differencesthe lack of ability to model uncertainties and to identify unknown parameters values, especially for coupled complex systems such as vehicles. Effects of unknown model parameters vary under different maneuvers and the ability to excite a source of uncertainty is the focus of this study. We propose an optimization method to generate a proper maneuver that maximize the sensitivity of uncertain parameters based on global sensitivity analysis (GSA). Sensitivities with respect to individual uncertain parameters and those that consider coupled effects are all included. We utilize Kriging-based metamodels to improve the efficiency of the GSA problems with computationally expensive simulations. The optimal design of excitation maneuvers to create the most sensitive performances can then be obtained. The applicability and the accuracy of the proposed method are assessed via a math model and a practical application on a x-by-wire autonomous tricycle. Results show that our proposed method can assist in providing a suitable maneuver as an alternative validation to uncertain parameters in a vehicle system.

Keywords: Excitation, Metamodel, Global Sensitivity Analysis, Uncertainty, Optimization, Vehicle System

*Corresponding author

1 INTRODUCTION

Complex systems such as manufacturing machinery, vehicles, and airplanes account for hundreds to thousands of subsystems with a total number of parameters in the order of tens of thousands. Among these parameters, some can be directly determined by on-site measurements such as geometric dimensions. Immeasurable parameters need to be estimated from performance outputs. Ideally each performance can guide us to a specific parameter value, however, real-world engineering system parameters are strongly coupled.

Validation in engineering identifies and quantifies the differences between simulation models and the reality. Well-validated models can predict the performance of a design in the concept stage. With the increase of system complexity, validating coupled subsystems presents an engineering challenge. Key model parameters should match in reality, especially when they are difficult to measure, if at all possible. Alternatively, the estimates of parameters are inferred from performance measurements when direct measurements are not available. Testing procedures, which are executed in model validation stage, should be able to show how the errors between simulation model and experimental data differ, and provide a constructive instruction for increasing model's confidence, such as adjustments on math and physics model or parameter identification.

Typical approaches in validating vehicle simulation models compare the performances of simulation models with the experimental data in a pre-defined testing maneuver [1], mostly following the standard performance criteria as defined by the International Organization of Standardization (ISO). For example, Setiawan validated a 14 Degree of freedom (DOF) vehicle model [2] using the well-correlated trend of simulation and experiment result of tire slip angle response from double lane change test [3]. Gawade validated a 6 DOF three-wheeled vehicle model by comparing the average radius difference in steady state circular test [4] to tell the accuracy of the built model [5]. Aside from ISO testing maneuvers, approaches created by researchers such as 180^o constant radius turn [6] and sinusoidal steer [7] on steering wheel are also used in practical cases. Engineers can only select the maneuver by intuition. For example, it is guessed that double lane change maneuver may enable high lateral acceleration and high values of tire sideslip angles [8], which may lead to loss of stability, so it might be suitable as a validation method. However, these cases only present the predictability of simulation model in the given situation, but few can deal with uncertainty classification and improvement of the model. In other words, these validating approaches, including ISO testing maneuvers, are accessing real vehicle performances rather than discussing the difference between both models. Methodical procedure in order to enhance the link between the experimental test data and validity analysis of simulation model is still lacking.

The ideas of exciting the effects on parameters to be observed are actually a popular techniques applied in many engineering fields. In vehicle engineering, sensor errors are excited by adjusting different strategies in overtaking [9], showing that differences in driving maneuver will impact the sensitivity of parameters on system's output. In identification of robot dynamic model, excitation trajectories [10, 11], which are a composition of fraction of spline curves, are designed by optimizing a two-weighted term fitness function, which is composed of a trajectory-forming matrix and a coupling index, and are able to identify inertial terms and parameters of friction model by using Least Square [12]. To identify aircraft parameters, a design method based on the wavelet transform was developed that allows to generate multi-axis input signals with the ability to specify both the frequency content and the times when the frequencies are excited, with as little parameters as possible. [13] and show that accurate aerodynamic parameters can be extracted from these multi-axis maneuvers. Optimum inputs which provide maximum possible accuracy of derivative estimates are to be found and parameters in longitudinal and lateral linear models of conventional aircraft are to be identified [14]. Techniques such as NExT (Natural Excitation Techniques) and PE (Persistent Excitation) [15] are widely used in system identification. Although few works are related to excitation of uncertain parameters in vehicle, we found that the common key points to generate the optimal ”trajectory”, or how we manipulate the system, are two: parameterize the input or trajectory so that it can be calculated by the algorithm, and quantify the coupling effect of parameters by an index which is able to be an optimized objective.

Parameterizing maneuvers for vehicle can be achieved with the X-by-wire techniques, for the input commands and executions can be precisely controlled while the control action are done by motors, especially for autonomous vehicles. Quantifying and classifying coupling effects can be done by global sensitivity analysis [16]. Global sensitivity analysis, which not only considers the contribution on a single factor, but also analyze the interaction effects, is a general and mature method in uncertainty analysis [17]. However, for complex systems like vehicle, the large amount of computation makes sampled-based sensitivity and uncertainty analysis almost impossible to be done [18]. Therefore, the concept of DACE (Design and Analysis of Computer Experiments) [19] is introduced in this work, and a metamodel-based sensitivity analysis method is utilized [20]. When sensitivity indices are calculated, optimization of excitation maneuvers can be realized.

This research aims to provide a systematic approach in observing model parameter values by changing operating parameters as in Eq. 1.

$$
\begin{aligned}
\text{Optimize} \quad & \text{Cost Function} \\
& (\text{operation parameters, model parameters}) \\
\text{w.r.t.} \quad & \text{operation parameters} \qquad (1) \\
\text{s.t.} \quad & \text{feasible operation given system parameter ranges}
\end{aligned}
$$

In Section 2, implementation details of realizing these techniques are explained. Applicability and accuracy assessments are presented by an illustrative math model in Section 3. In Section 4, details of our vehicle systems are described.Section 5 will demonstrate the application on generating excitation maneuver on tire parameters of a tadpole designed three-wheeled vehicle as an engineering case. At last, Section 6 concludes the study with a glimpse on using global sensitivity analysis to identify the specific unknown model parameters by optimizing excitation maneuvers.

2 Proposed Method for Optimal Excitation Maneuvers

In what follows, let us define Eq. 2 as a general system with operation parameters $\mathbf{x}$ and model parameters $\mathbf{p}$. Without loss of generality, we assume that all measurable and known parameters are treated as constants in Eq. 2. $\mathbf{p}$ in Eq. 2 are k-dimensional unknown parameters to be identified. $\mathbf{m}$ in Eq. 2 is the generalized system output.

$$f(\mathbf{x},\mathbf{p}) = \mathbf{m} \qquad (2)$$

By following this form, excitation operation on p_i can be generally described as Eq. 3, meaning that the effect of deviation of p_i is maximized under operating $\mathbf{x}^*$.

$$\mathbf{x}^* = \arg\max \frac{\partial f}{\partial p_i} \tag{3}$$

The flowchart of the proposed method of optimal excitation maneuvers can be seen in Fig. 1 with 2 stages : metamodel-based sensitivity analysis and excitation maneuver optimization.

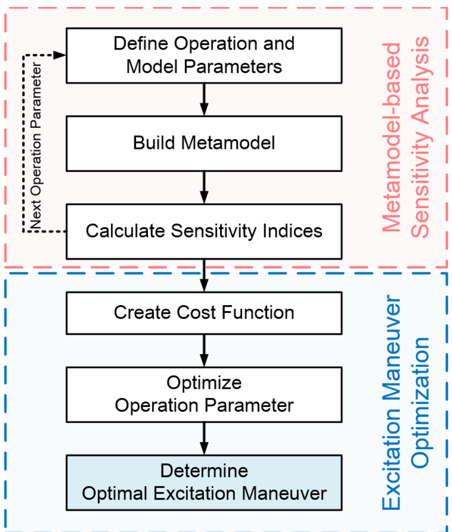

FIGURE 1. Flowchart of the proposed method

Metamodel-based sensitivity analysis aims to build cheaper replacements (Kriging metamodels) of f, denoted as $\hat{f}(\mathbf{x}_j, \mathbf{p})$, with respect to all $\mathbf{p}$ at a given operation $\mathbf{x}_j$. Sobol method is then used to calculate the sensitivity of $\hat{f}$ with respect to $\mathbf{p}$ denoted as S_i, the main sensitivity index, and S_i^t as the total sensitivity, for p_i. When operation parameters, $\mathbf{x}$ with dimension l, change, a c-level of full factorial design is performed. Therefore the metamodeling-based sensitivity analysis builds c^l Kriging models. The second stage in Fig. 1 builds additional Kriging models with operation parameters as inputs and each sensitivity index as output, denoted as $\hat{S}_{p_i} = \hat{F}_{m_i}(\mathbf{x})$ and $\hat{S}^t_{p_i} = \hat{F}_{t_i}(\mathbf{x})$ that will then be used in an optimization framework to obtain the optimal operating maneuvers $\mathbf{x}^*$ for parameter identification.

2.1 Metamodel Building

Building a metamodel consists of sampling and fitting. Details of our method with initial sampling and Kriging modeling with efficient global optimization (EGO) is listed in Algorithm 1.

Algorithm 1 Steps for building Kriging metamodels

procedure BUILD INITIAL KRIGING MODEL
  $\mathbf{x}_j \leftarrow$ Selected operation parameters
  $\mathbf{p_0} \leftarrow k$-dimensional Sobol sequence with N_{initial} samples
  $\mathbf{m_0} = f(\mathbf{x}, \mathbf{p_0}) \leftarrow$ Simulation output vectors
  $\hat{f}_0 = Krig(\mathbf{p_0}, \mathbf{m_0}) \leftarrow$ Fit Kriging model
procedure REFINE KRIGING MODELS USING EGO
  while $ISC_{var}(\hat{f}) > Converge\ var.$ **do**
    $\mathbf{p}^* = \arg\max ISC_{var}(\hat{f})$
    $\mathbf{m}^* = f(\mathbf{x}_j, \mathbf{p}^*)$
    $\mathbf{p_0} = \{\mathbf{p_0}, \mathbf{p}^*\}$
    $\mathbf{m_0} = \{\mathbf{m_0}, \mathbf{m}^*\}$
    $\hat{f}_j = Krig(\mathbf{p_0}, \mathbf{m_0})$
  end

For unknown parameters $\mathbf{p}$, whose possible range are defined, it is assumed that the probability of existing are uniformly distributed within their own possible range. Therefore, N_{initial} initial Sobol sequence samples [21] are obtained and simulated. These data are then fitted using Kriging model to capture the nonlinearity and sparsity of the system with high robustness [20, 22, 23]. To enhance the precision of Kriging model with limited samples, efficient global optimization(EGO) technique is applied. Details of the EGO procedure are discussed in Refs. [22] and [24].

2.2 Sobol Sensitivity Indices

Variance-based method, also known as Sobol method, decompose the variance of a function, V, into the main term, V_i, and an increasing order of interaction terms, as in Eq. 4 [9, 25].

$$V = \left(\sum_{i=1}^{k} V_i\right) + \left(\sum_{i_1=1}^{k}\sum_{i_2=i_1+1}^{k} V_{i_1,i_2}\right) + \left(\sum\sum\sum V_{i_1,i_2,i_3}\right) \ldots + \left(V_{1,\ldots,k}\right) \tag{4}$$

The global sensitivity index is defined as the partial variance contributed by an effect of interest normalized by the total variance V as in Eq. (5).

$$S_{i_1 \ldots i_s} = V_{i_1 \ldots i_s}/V \tag{5}$$

The sensitivity with respect to a single parameter p_i is called *main sensitivity index* (MSI), and one corresponds with two or more variables ($S_{i_1 \ldots i_s} \forall s \geq 2$) is called *interaction sensitivity index* (ISI). The total influence of p_i induced by both the main and the interaction effects is defined as the *total sensitivity index* (TSI) as in Eq. 6

$$S_i^t = S_i + \widehat{S}_{i,\sim i} = 1 - \widehat{S}_{\sim i} \tag{6}$$

where $\widehat{S}_{i,\sim i}$ is the sum of all the $S_{i_1 \dots i_s}$ that involve with the index i and at least one index from $(1, \dots, i-1, i+1, \dots, k)$; $\widehat{S}_{\sim i}$ is the sum of all the $S_{i_1 \dots i_s}$ term that do not involve with index i.

The analytical approach to calculate these indices involves evaluating a set of multi-dimensional integrals [25], or reconstruct the ANOVA form of variance into results of univariate integrals expressed by tensor-product basis function (TPBF) [26]. Although these approaches can provide a precise estimation on indices, they are unsuitable to complex systems, such as vehicles. We take advantage of the Kriging models and use Monte-Carlo method to calculate the sensitivity [27]. Consider k parameters with N sample sets, we generate a the following matrix with Sobol sequence in Eq. 7, where the matrics $\mathbf{P}$ and $\mathbf{Q}$ are

$$\mathbf{P} = \begin{bmatrix}\mathbf{P}_1 \dots \mathbf{P}_k\end{bmatrix} = \begin{bmatrix} p_{1,1} & \cdots & p_{1,k} \\ p_{2,1} & \cdots & p_{2,k} \\ \cdots & \cdots & \cdots \\ p_{N,1} & \cdots & p_{N,k} \end{bmatrix}$$

$$\mathbf{Q} = \begin{bmatrix}\mathbf{Q}_1 \dots \mathbf{Q}_k\end{bmatrix} = \begin{bmatrix} p_{1,k+1} & \cdots & p_{1,2k} \\ p_{2,k+1} & \cdots & p_{2,2k} \\ \cdots & \cdots & \cdots \\ p_{N,k+1} & \cdots & p_{N,2k} \end{bmatrix} \tag{7}$$

Let us build the matrix $\mathbf{R}^i$ for $i = 1, 2, \dots k$ such that the ith column of $\mathbf{R}^i$ is equal to the ith column of $\mathbf{Q}$, and the remaining columns are copies of $\mathbf{P}$ as in Eq. 8.

$$\mathbf{R}^i = \begin{bmatrix}\mathbf{P}_1, \cdots, \mathbf{Q}_i, \cdots, \mathbf{P}_k\end{bmatrix} \tag{8}$$

By taking samples through all rows of matrix $\mathbf{P}, \mathbf{Q}, \mathbf{R}$, Sobol indices can be calculated by the concept of expected value and variance as in Eq. (9). $g(\mathbf{P})$, $g(\mathbf{Q})$, and $g(\mathbf{R})$ in Eq. 9 are the outputs of the system with corresponding input from sample matrix. With these definitions, the Sobol main effect index, S_j, can be calculated from Eq. 9 and the Sobol total effect index, S_i^t, can be calculated from Eq. 10:

$$S_i = \frac{var(E(g|p_i))}{var(g)} = \frac{\frac{1}{N}\sum_{u=1}^{N} g(\mathbf{Q})_u (g(\mathbf{R^i})_u - g(\mathbf{P})_u)}{\frac{1}{N}\sum_{u=1}^{N}(g(\mathbf{P})_u)^2 - (\frac{1}{N}\sum_{u=1}^{N} g(\mathbf{P})_u)^2} \tag{9}$$

$$S_i^t = \frac{var(E(g|p_{\sim i}))}{var(g)} = \frac{\frac{1}{2N}\sum_{u=1}^{N}(g(\mathbf{P})_u - g(\mathbf{R^i})_u)^2}{\frac{1}{N}\sum_{u=1}^{N}(g(\mathbf{P})_u)^2 - (\frac{1}{N}\sum_{u=1}^{N} g(\mathbf{P})_u)^2} \tag{10}$$

2.3 Cost Function Development

We can see from Eq. 3 that the target of sensitivity analysis is to understand in what ways and by how much the output vector $\mathbf{m}$ is influenced by $\mathbf{p}$. Before the values of $\mathbf{p}$ are identified, let us use $F(\mathbf{x}_j)$ as a representation in generating sensitivity, as shown in Fig. 2.

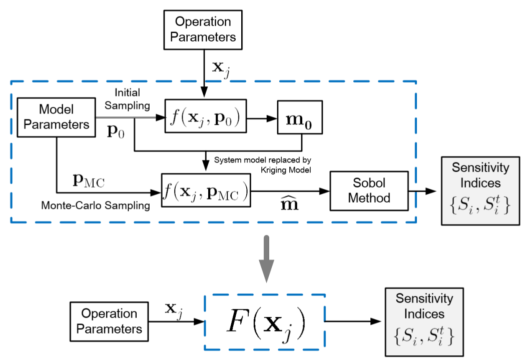

FIGURE 2. Simplification of Metamodel-based sensitivity analysis process: From the flowchart, we can see that sensitivity indices are a function of operation parameters.

The core of designing the optimal excitation maneuver is to maximize the main effect of single parameter such that the parameters can easily be estimated. We define a cost function H_p of Sobol indices, as in Eq. 11.

$$H_p(S_1 \dots S_k, S_1^t \dots S_k^t) = \frac{S_i^t - S_i}{S_i} + \frac{S_1 + \dots + S_k - S_i}{S_i} \tag{11}$$

Eq. 11 shows the cost function for operation parameters to excite model parameters p_i. The first term sums all the interaction effect involves with p_i, and the second term is the sum of main effect indices with S_i excluded. Therefore, this cost function can fully express the spirit of model parameter excitation.

2.4 Excitation Maneuver Optimization

With the constructed cost function, the optimization problem in this work can be written in general format, as in Eq. 12.

$$
\begin{aligned}
\min \quad & H_p(\mathbf{S},\mathbf{S^t}) = \frac{\hat{S}_i^t - \hat{S}_i}{\hat{S}_i} + \frac{\hat{S}_1 + \hat{S}_2 + \ldots + \hat{S}_k - \hat{S}_i}{\hat{S}_i} \\
\text{w.r.t} \quad & \mathbf{x} \\
\text{s.t.} \quad & \hat{S}_i = \hat{F}_{m_i}(\mathbf{x}), i = 1, \ldots, k \\
& \hat{S}_i^t = \hat{F}_{t_i}(\mathbf{x}), i = 1, \ldots, k \\
& \forall\{\mathbf{x},\mathbf{p}\} \in \mathscr{F}
\end{aligned} \tag{12}
$$

Note that $\hat{F}_{m_i}$ and $\hat{F}_{t_i}$ are Kriging models in obtaining main and total sensitivity, respectively. Details of how these surrogate models are created can be seen from Fig. 3. Each of the sampling $\mathbf{x}_j$ is a vector describing the jth maneuver. $\mathscr{F}$ represent the overall feasible space of $\mathbf{x}$ and $\mathbf{p}$.

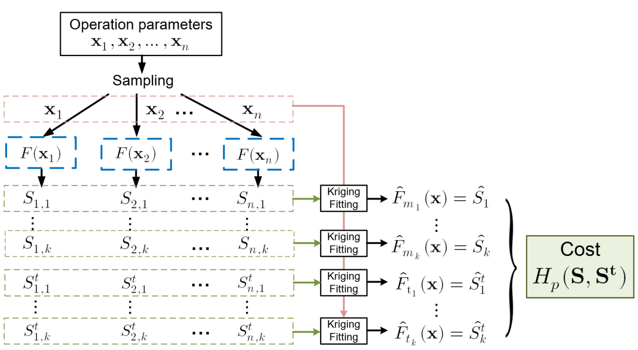

FIGURE 3. Derivation of cost function: This flowchart shows that the cost function is composed of sensitivity indices which are functions of $\mathbf{x}$, and thus we can derive the cost function as a function of $\mathbf{x}$ also.

In this derivation, n samples are taken in the l-dimensional design space of $\mathbf{x}$, noting $\mathbf{x}_j, j = 1 \sim n$. After sampling, Kriging models $\hat{F}_{m_i}(\mathbf{x})$ and $\hat{F}_{t_i}(\mathbf{x})$ are used to connect the relationship between sampling points of $\mathbf{x}$ and each calculated sensitivity index $\{S_i, S_i^t\}, i = 1, \ldots, k$, which means $2k$ Kriging model will be fitted for every $\mathbf{x}$'s main and total index. With these steps, cost function can be established by combination of Kriging models.

At last, the simplified $H_p(\mathbf{x})$ can be easily estimated by any given $\mathbf{x}$ without undergoing the whole computations, which makes the optimization algorithm more efficient. Therefore, in this work, $\mathbf{x}^*$ can be estimated straightforwardly by global searching on Kriging models with `DIRECT` algorithm [28].

3 An Illustrative Analytical Example

3.1 Design Space and Flowchart

In this section we consider the function in Eq. 13 with four variables [26]. The operation parameters x_i, $i = 1,2,3,4$ and α are within the ranges of $-5 \le x_1, x_2, x_3, x_4 \le 0$ and $\alpha = 1$. p_i, $i = 1,2,3,4$ are model parameters are assumed to be within $0 \le p_1, p_2, p_3, p_4 \le 1$.

$$
\begin{aligned}
f(x) = \alpha_1 &+ e^{x_1[(p_1-1)^2+p_2^2]+x_2(p_3^2+p_4^2)} \\
&+ e^{x_3[(p_2-1)^2+p_1^2]+x_4(p_3^2+p_4^2)}
\end{aligned} \tag{13}
$$

Flowchart of implementation on math model is shown in Fig. 4. Details of $F(\mathbf{x})$ and $H_p(\mathbf{x})$ can be found in section 2.3 and 2.4 relatively.

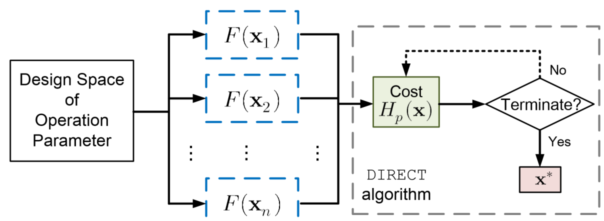

FIGURE 4. Flowchart of math model implementation

Enough samples (Usually 10 times of design variables, in this case $n = 96$) samples are taken from the $l = 4$ dimensional design space of $\mathbf{x}$ by Sobol sequence in fitting $H_p(\mathbf{x})$.

3.2 Accuracy Assessment of Kriging Model Fitting

Setting $x_1, x_2, x_3.x_4 = [-0.5, -2, -0.5, -2]$, 1000 random samples are of $\mathbf{p}$ are taken as the training set to fit Kriging model, and an additional 10000 samples are taken as validation set to evaluate the estimation error. The distributions of estimation errors as shown in Fig. 5 with mean $\mu_e = 1.64e-5$ and standard deviation $\sigma_e = 3.70e-7$. The assessment indices are $R^2 = 0.99997$ and $RAAE = 0.0019$ [20].

3.3 Accuracy Assessment of Monte Carlo Method on Sobol Sensitivity Indices

The Sobol indices with sensitivities calculated from N Monte Carlo samples might vary [26], as shown in Table 1. N should be rationally large enough to ensure converged indices.

Computer experiments are done by substituting different sample number N, and the results are compared with the analytical solution in [26]. The results in Fig. 6 show that estimation of Sobol indices converges when N is larger than $5e5$ with estimation errors between 0.0005 to 0.002.

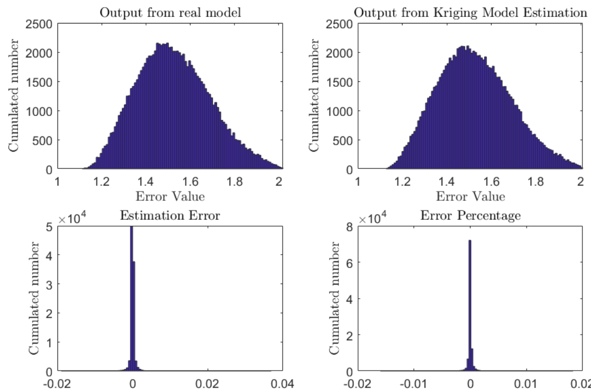

FIGURE 5. Error distribution of Kriging model estimation

TABLE 1. Comparison between calculated indices by analytical approach and Monte Carlo Method, $\{x_1 = -2,\ x_2 = -0.5,\ x_3 = -2,\ x_4 = -0.5,\ \alpha_1 = 1\}$

	(S_1, S_1^t)	(S_2, S_2^t)	(S_3, S_3^t)	(S_4, S_4^t)
Analytical Method	(0.0033, 0.5798)	(0.0033, 0.5798)	(0.2063, 0.2220)	(0.2063, 0.2220)
$N = 100,000$	(0.0208, 0.5820)	(0.0089, 0.5838)	(0.2126, 0.2235)	(0.2326, 0.2216)
$N = 10,000$	(0.0787, 0.5809)	(0.0518, 0.5835)	(0.2126, 0.2235)	(0.2326, 0.2216)
$N = 1000$	(0.2448, 0.6119)	(0.3761, 0.6167)	(0.4844, 0.2225)	(0.2814, 0.2467)

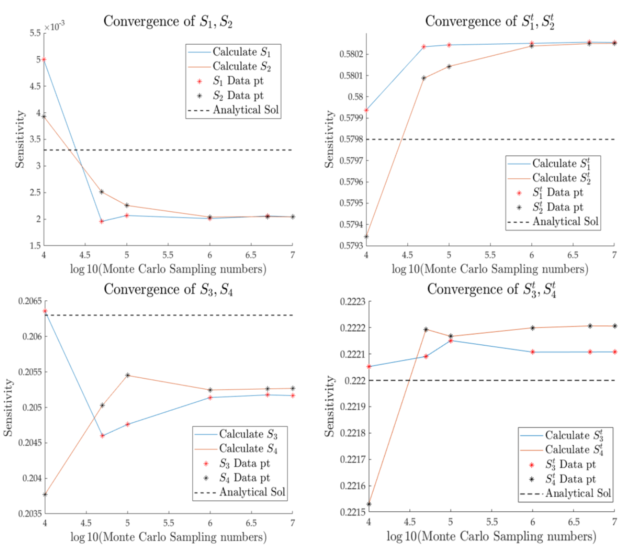

FIGURE 6. Convergence of Sobol indices at different sample sizes

3.4 Results Verification

To evaluate the accuracy of optimization results, the optimization procedure without building Kriging models, shown in Fig. 7, is conducted. $F(x)$ and the cost function H_p are both obtained directly by math model and the Sobol indices that are calculated directly in each iteration of `DIRECT` algorithm. Although the verification is not suitable for complex systems, it is used only to ensure the validity of the proposed method .

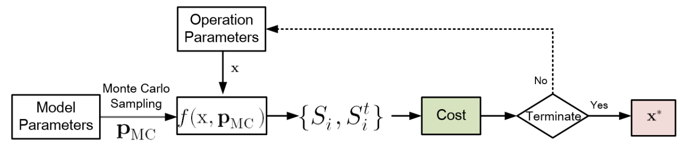

FIGURE 7. Direct approach of optimizing system parameters

Fig. 8 shows how the algorithm finds the optimum and the result difference between two algorithms. Main Sensitivity Indices (MSI) and Total Sensitivity Indices (TSI) while exciting p_1, p_2 and p_3, p_4 are plot in Fig. 9. Due to the symmetrical location of p_1, p_2 and p_3, p_4, their effect and optimum should be identical as well, and meaning that the coupling scenario cannot be easily decouple by this method.

Although the existence of estimation bias between two approaches, especially while observing p_3 and p_4, the answer from Kriging optimization is still considered to be usable for the correct trend and acceptable inaccuracies. As a conclusion, adjustment of system parameters can change main and total effects of design parameters, and excitation can be realized by optimizing the given cost function. Also, coupling of design variables can be observed from this process. Therefore, the proposed method is verified and demonstrated by this math model, and it is believed to be applicable on complex systems.

4 Details of the Vehicle System

An X-by-wire tricycle was developed as a cheaper test-bed, as shown in Fig. 10(a), a more sophisticated vehicle systems as the target to be analyzed. The main hardware of its structure consists of three bicycle frame that compatible with 26×1.65 tires. With an 1.43 (m) wheelbase, a 0.62 (m) front-track, and weighing 48.3 (kg), the tricycle is driven by an 48V, 250W in-wheeled motor on the single rear wheel and can achieve maximum speed around 17 km/hr. The steering system includes a symmetric 6 links and 7 joints mechanism driven by a servo motor that varies the δ_R/δ_L ratio from 0.8 to 0.6 with steering motor input between $0°$ to $45°$, and a $20°$ positive caster angle.The vehicle control unit is based on an NVIDIA Jetson TX2 on ROS. PLCs for steer-by-wire and drive-by-wire subsystems are built by Arduino UNO. The X-by-wire tricycle with transparent structure and components allows experiments to be executed in precision.

The dynamic model of the tricycle is built on Simulink as shown in Fig. 10(b) that include characteristics of both four-wheel vehicle and two-wheel motorcycles for parameters

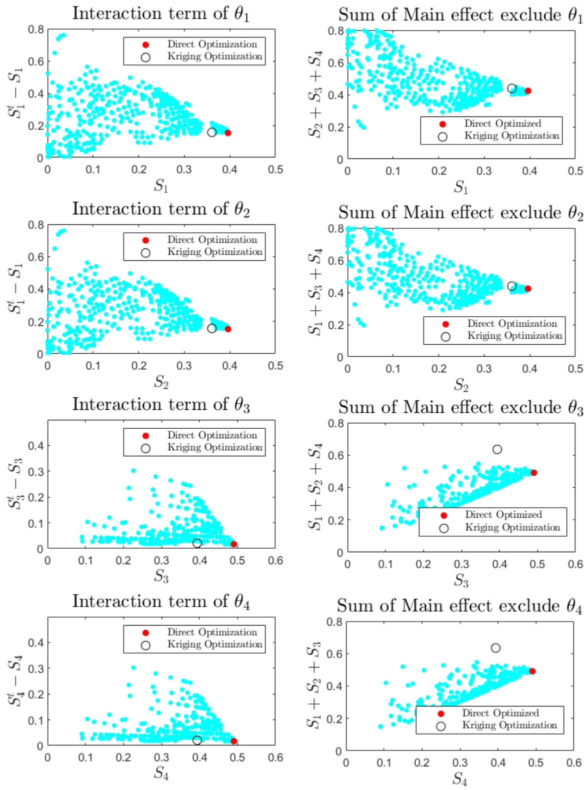

FIGURE 8. Result of optimizing cost of math model

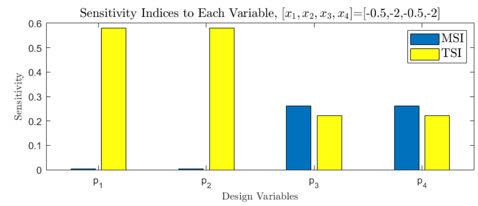

(a) Sensitivity Indices of default parameters

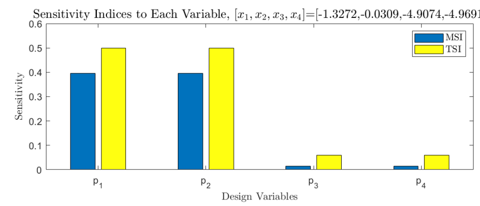

(b) Exciting p_1, p_2 by Direct approach

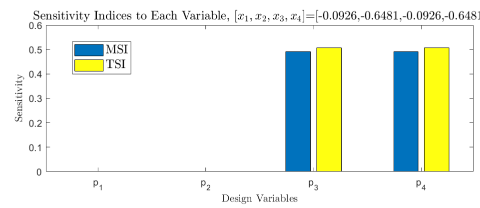

(c) Exciting p_3, p_4 by Direct approach

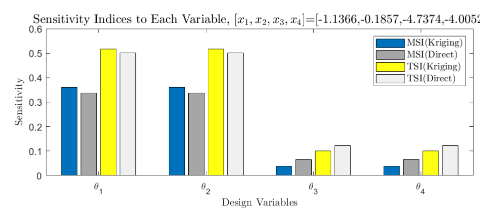

(d) Exciting p_1, p_2 by Kriging approach with validation

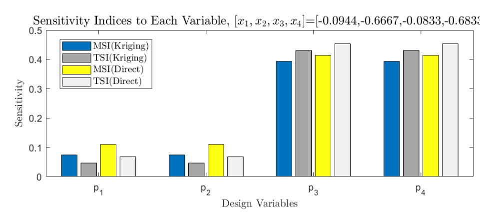

(e) Exciting p_3, p_4 by Kriging approach with validation

FIGURE 9. Sensitivity Indice with different system parameters

such as caster angle in the steering mechanism, and camber angle [29–32]. The tricycle's parameters are divided into model parameters and operation parameters. Six model parameters $\mathbf{p} = p_1, \ldots p_6$, listed in Table2, are unknowns to be determined. Other key specifications determining the performance of this vehicle are directly measurable and therefore treated as constants in our study.

Operation parameters define and form a unique maneuver with drive and steer commands for vehicles during path following. In this study, we use the geometry of a path as an alternative of a unique maneuver. The optimal excitation maneuvers obtain the best operation parameters that are considered as the design variable $\mathbf{x}$ in the study. This study focuses on two maneuvers: double lane change and steady state circular maneuver. A double lane change maneuver can be modeled via Bézier curves with the control points $P_0, \ldots P_3$ as shown in Fig. 11 [33]. d_1 and d_2 are assigned as the design variables $x_1 = d_1 = [0,8], x_2 = d_2 = [0,8]$ that determine different lane change strategies. A steady state circular maneuver is defined by a path radius $x_1 = r_d = [2,6]$ and a target velocity $x_2 = v = [0.6, 0.1]$. Details on selecting the optimal system parameters for generating excitation trajectories will be in Section 5.

5 DESIGN OF EXCITATION MANEUVERS FOR VEHICLES

The proposed method on designing excitation maneuvers is applied to the aforementioned tricycle in this section. Fig. 12 provides the details of the entire process in this study. Two operation parameters $\{x_1, x_2\}$ define the both the double lane change and the steady state circular maneuvers, and two unknown model parameters, cornering stiffness and camber

(a) Tadpole design three-wheeled vehicle

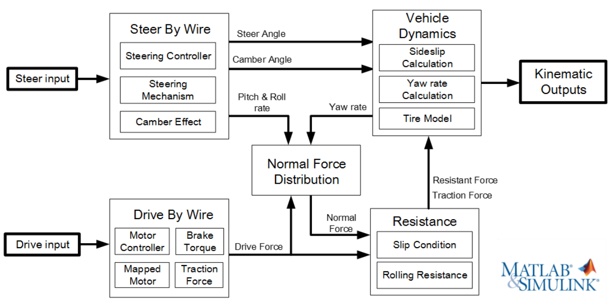

(b) 9 DOF Vehicle Dynamic Model in Simulink

FIGURE 10. Vehicle Model

TABLE 2. Specification of vehicle model

Fixed Parameters (Partial)			
item	value(unit)	item	value(unit)
Front wheel to COM	0.724(m)	Wheelbase	1.43(m)
Rear wheel to COM	0.719(m)	Total mass	48.3(kg)
Left wheel to COM	0.3065(m)	Tire radius	0.335(m)
Right wheel to COM	0.3135(m)	$I_{front\ wheel}$	0.3(kgm^2)
Ground to COM	0.4896(m)	$I_{rear\ wheel}$	0.5(kgm^2)
I_{xx}	12.1(kgm^2)	I_{yy}	36.7(kgm^2)
Unknown Parameter			
Cornering Stiffness	500-1500 (N/rad)	Camber Stiffness	25-75 (N/rad)
SAP	0-0.3 (N.m/rad)	I_{zz}	25-75 (kgm^2)
Rolling Coefficient 1	0.0045-0.0135 (N/m^2)	Rolling Coefficient 2	0.00025-0.00075 (N/m^4)

stiffness noted as $\mathbf{p} = \{p_1, p_2\}$, are our main focus.

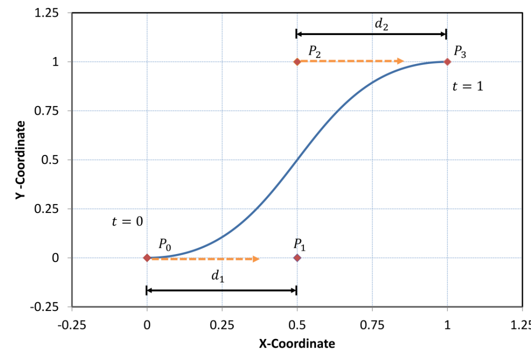

FIGURE 11. The 3^{th} order S-shaped Bézier curve [9]

5.1 Trajectory Deviations

Trajectory Deviation are assigned as the model output in this case. We assume that the deviations in model parameters $\mathbf{p}$ are the only sources of uncertainty that contributes the output difference compared with real model. Since each vehicle performance constitute a time-velocity profile, $\mathbf{m}$ is in vector, the sum of square error (SSE) between two $\mathbf{m}$ outputs is used as the scalar index representing differences between two trajectories.

As shown in Fig. 12, the nominal values of model parameters $\mathbf{p}_0$ and the the path generated from the operation parameters are provided to the Simulink model. Each output is represented by location points on the trajectory in global axis as $\mathbf{m^0} = \{x_1^0, ...x_t^0;\ y_1^0, ..., y_t^0\}$. We use 10 thousand discrete points, $t = 10,000$, to present the continuous trajectory and the corresponding steering and driving commands are obtained. Once we have the nominal driving situations, initial samples with size $N_{\text{initial}} = 4000$ on the model parameters are taken randomly from a predetermined uniform distribution. Executing all 4000 simulations gives us the error index of each trajectory from Eq. 14.

$$TE^i = \frac{1}{k}\left(\sum_{j=1}^{k}(x_j^i - x_j^0)^2 + (y_j^i - y_j^0)^2\right),\ i = 1, 2, ...N_{\text{initial}} \quad (14)$$

TE in Eq. 14, the trajectory error index, are the selected as the output while samples of $\mathbf{p}$ are the input the Kriging model. EGO are activate if maximum variance of Kriging model are larger than 0.01 times the mean of Kriging model and total sampling number is less than 4200. With these process, a sensitivity analysis and optimization can be done by the identical process mentioned in Section 3.

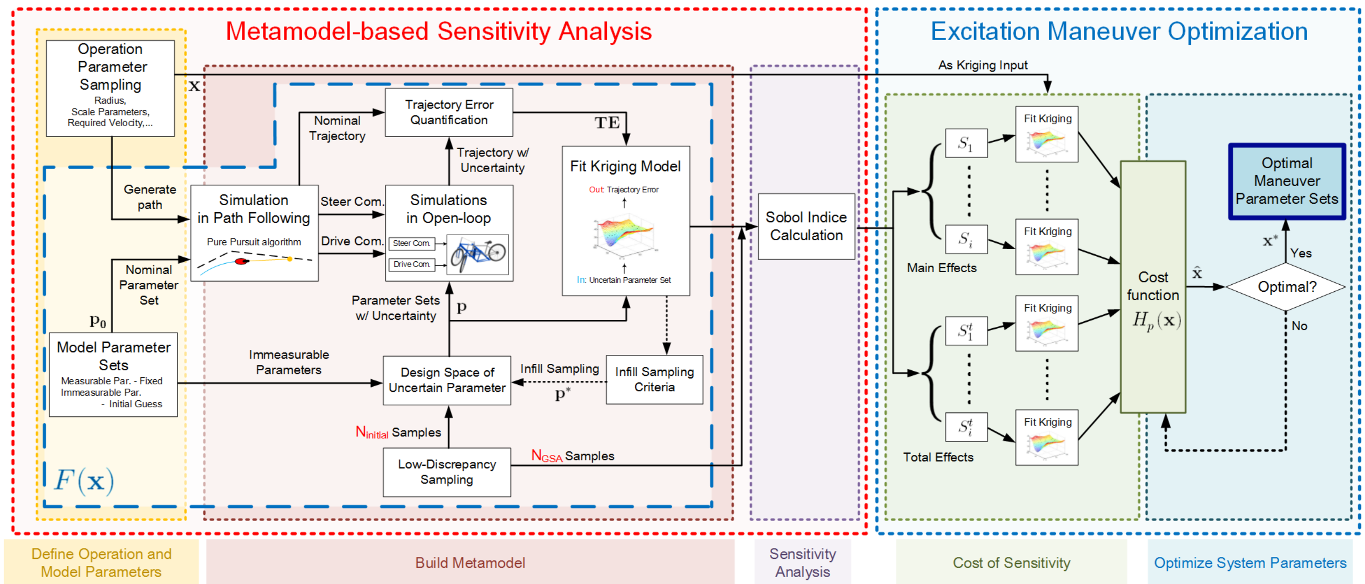

FIGURE 12. Flowchart on generating excitation maneuver for vehicle

5.2 Metamodel Accuracy Assessment

Fig. 13 shows the mean and standard deviation of of estimation errors with mean $\mu_e = 9.0876$ and standard deviation $\sigma_e = 20.1165$ with $R^2 = 0.9145$ and $RAAE = 0.1030$ when $\mathbf{p} = [2,2]$ in double lane change maneuver. We believe that this model are suitable and has enough confidence to be the replacement of the Simulink model.

5.3 Optimization Result

Sensitivity analysis shows that the cornering stiffness α and camber stiffness β nearly contribute to all of the output variance. The excitation of these two parameters are demonstrated. Results of exciting impacts of cornering stiffness and camber stiffness under steady state circular maneuver and double lane change maneuver are presented by MSI and TSI in Fig. 14 and Fig. 15, respectively. A point with randomly operation parameter is also shown in these figures as comparisons. From the plots we can see that the main effect of excitation target are magnified, while those of others are reduced as much as possible. In Fig. 16, trajectories of models with different model parameters are shown, which are simulated with a random-picked operation and the designed ones respectively. The figures show that the difference in the two model are more obvious when models are driven by the designed operation. Under this circumstance, parameter difference are more easier to be detected, leading to a better tuning and model calibration.

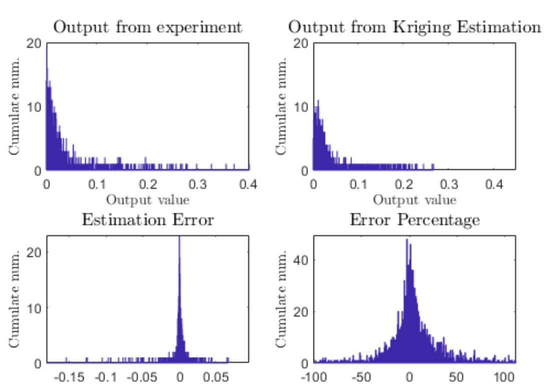

FIGURE 13. Error distribution from Kriging model estimation of TE

From the optimization processes in (Fig. 17 and Fig. 18), we can confirm that the results not only are reasonable but are also the the optimum that can maximize the identifiability. Based on the observed results, we can conclude that that the proposed method can help the X-by-wire tricycle identifying the impacts due to tire cornering and camber stiffness in both lane-change and steady-state circular maneuvers.

6 Closure

A novel approach on designing unknown parameter excitation trajectory for an X-by wire tricycle are proposed in this paper. By applying metamodel techniques, sensitivity analysis and optimization can be done to determine the maneuver that magnified the effect of observe target while the couple effect are minimized. Quantification and classification of

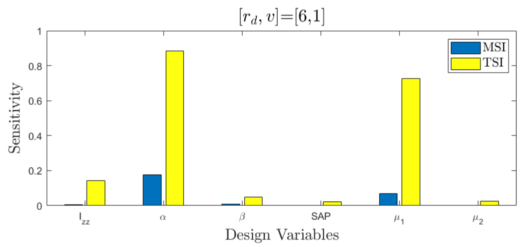

(a) Sensitivity indices of random selected operation parameters

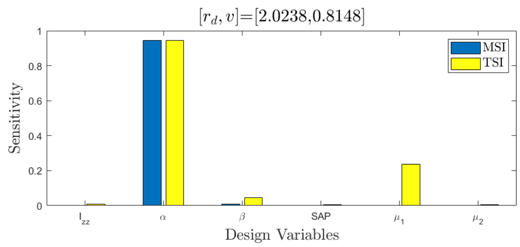

(b) Sensitivity indices when exciting cornering stiffness

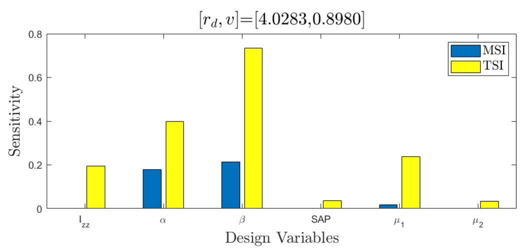

(c) Sensitivity indices when exciting camber stiffness

FIGURE 14. Sensitivity indices with optimal operation parameters on steady state circular maneuver

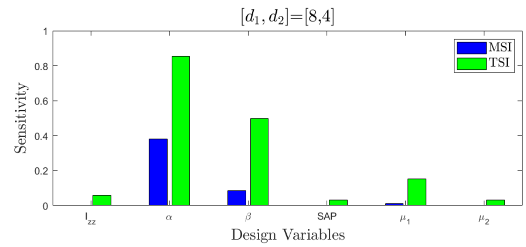

(a) Sensitivity indices of random selected operation parameter

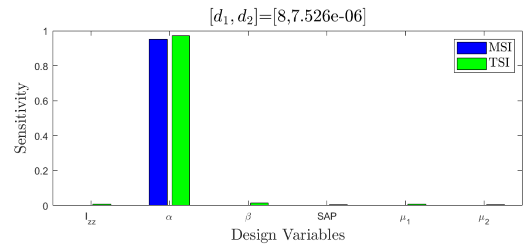

(b) Sensitivity indices when exciting cornering stiffness

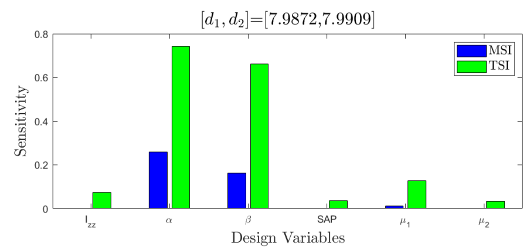

(c) Sensitivity indices when exciting camber stiffness

FIGURE 15. Sensitivity indices with optimal operation parameters on double lane change maneuver

uncertainties, which assist in determination of significant parameters and observations of coupling effect, are demonstrated during the process. The proposed method is applied to a math model to verify that the optimal system parameters can be obtained. It is also applied to generate excitation maneuvers for a tricycle in our research. The results show that proper operation parameters are designed to excite cornering stiffness and camber stiffness in two maneuvers, meaning that the systematic process proposed in this work is worth implementing.

The extended goals of providing excitation maneuvers lie on the identifications of unknown model parameters. Among all these parameters, in many cases the parameters that are difficult to be measured are the ones of critical importance. Therefore one can expect that the excited performance reveal the hidden values of these unknown parameters. We set the objective to identify unknown parameter the goal of our future research mig

List of Symbols

f	The system model as a function of $\mathbf{x}$ and $\mathbf{p}$
$\hat{f}$	The metamodel of f
$\hat{f}_j$	The metamodel of f at a fixed $\mathbf{x}_j$
$F(\mathbf{x})$	A simplified function of x_i that calculates MSI and TSI
$\hat{F}_{m_i}(\mathbf{x})$	A Kriging model that estimates MSI of p_i under any $\mathbf{x}$, fitted from $\mathbf{x}$ as the input and all the S_i from $H(\mathbf{x}_j)$ as the output. $i=1\sim k, j=1\sim n$
$\hat{F}_{t_i}(\mathbf{x})$	A Kriging model that estimates TSI of p_i under any $\mathbf{x}$, fitted from $\mathbf{x}$ as the input and all the S_i^t from $H(\mathbf{x}_j)$ as the output. $i=1\sim k, j=1\sim n$
$H_p(\mathbf{S},\mathbf{S^t})$	Cost function composed of all the MSI and TSI of every $p_i, i=1\sim k$
$\mathbf{m}$	The vector output of $f(\mathbf{x},\mathbf{p})$
$\hat{\mathbf{m}}$	Vector outputs from $\hat{f}_j(\mathbf{x},\mathbf{p}_{MC})$
N	The sample size of $\mathbf{p}$
$\mathbf{p}$	The set of model parameters with size k
S_i	The main sensitivity index (MSI) of p_i
S_i^t	The total sensitivity index (TSI) of p_i
$\hat{S}_i$	Estimated MSI of p_i from $H_{m_i}(\mathbf{x})$

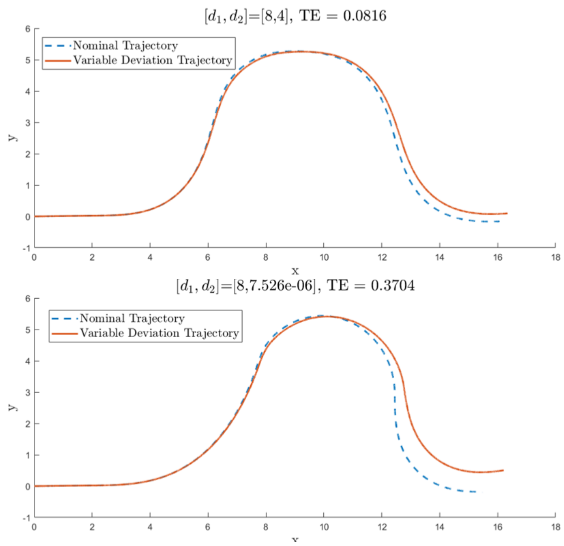

(a) Random-picked and designed double change maneuver

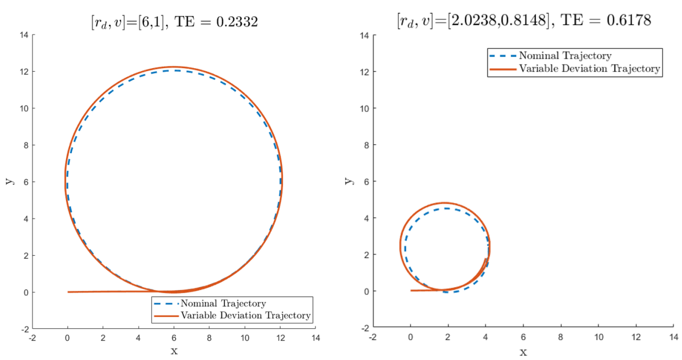

(b) Random-picked and designed steady state circular maneuver

FIGURE 16. Trajectory comparison on exciting cornering stiffness

$\hat{S}_i^t$	Estimated TSI of p_i from $H_{t_i}(\mathbf{x})$
$\mathbf{S}$	The vector of all MSI, $S[i] = S_i$, of size k
$\mathbf{S^t}$	The vector of all TSI, $S^t[i] = S_i^t$ of size k
$\mathbf{x}_i$	The ith set of operation parameters with size l

REFERENCES

[1] E. Kutluay and H. Winner. Validation of vehicle dynamics simulation models - A review. *Vehicle System Dynamics*, 52(2):186–200, 2014.

[2] E. Kutluay and H. Winner. Assessment methodology for validation of vehicle dynamics simulations using double lane change maneuver. *Proceedings - Winter Simulation Conference*, pages 3180–3191, 2012.

[3] Passenger cars — test track for a severe lane-change manoeuvre — part 1: Double lane-change. Standard, International Organization for Standardization, Geneva, CH, March 2018.

[4] Steady-state circular driving behaviour — open-loop test methods. Standard, International Organization for Standardization, Geneva, CH, June 2012.

[5] T.R. Gawade, S. Mukherjee, and D. Mohan. Six-degree-of-freedom three-wheeled-vehicle model validation. *Proceedings of The Institution of Mechanical Engineers Part D-journal of Automobile Engineering - PROC INST MECH ENG D-J AUTO*, 219:487–498, 04 2005.

[6] S. Yang and J. Kim. Validation of the 6-dof vehicle dynamics model and its related vba program under the constant radius turn manoeuvre. *International Journal of Automotive Technology*, 13, 06 2012.

[7] R. W. Allen, T. J. Rosenthal, D. H. Klyde, K. J. Owens, and H. T. Szostak. Validation of ground vehicle computer simulations developed fordynamics stability analysis. In *International Congress & Exposition*. SAE International, feb 1992.

[8] M. Wielitzka, A. Busch, M. Dagen, and T. Ortmaier. Unscented Kalman Filter for State and Parameter Estimation in Vehicle Dynamics. *Kalman Filters - Theory for Advanced Applications*, 2018.

[9] H. Tsai. Analysis the impact of sensing error for vehicle overtaking maneuver using global sensitivity. Master's thesis, National Taiwan University, 2019.

[10] E. Villagrossi, G. Legnani, N. Pedrocchi, F. Vicentini, L. M. Tosatti, F. Abbà, and A. Bottero. Robot dynamic model identification through excitation trajectories minimizing the correlation influence among essential parameters. *ICINCO 2014 - Proceedings of the 11th International Conference on Informatics in Control, Automation and Robotics*, 2(January 2016):475–482, 2014.

[11] G. Calefiore, M. Indri, and B. Bona. Robot dynamic calibration: Optimal excitation trajectories and experimental parameter estimation. *Journal of Robotic Systems*, 18(2):55–68, 2001.

[12] C. Presse and M. Gautier. New criteria of exciting trajectories for robot identification. In *Proceedings IEEE International Conference on Robotics and Automation*, pages 907–912 vol.3, May 1993.

[13] M. S. Roeser. Multi-axis maneuver design for aircraft parameter estimation. In *Deutscher Luft-und Raumfahrtkongress*, 2018.

[14] W. Wells and S. Ramachandran. Multiple control input design for identification of light aircraft. *IEEE Transactions on Automatic Control*, 22(6):985–987, December 1977.

[15] K. S. Narendra and A. M. Annaswamy. Persistent excitation in adaptive systems. *International Journal of Control*, 45(1):127–160, 1987.

[16] J. D. Salciccioli, Y. Crutain, M. Komorowski, and D. C. Marshall. *Sensitivity Analysis and Model Validation*, pages 263–271. Springer International Publishing, Cham, 2016.

[17] A. Saltelli, S. Tarantola, and KP-S Chan. A quantitative

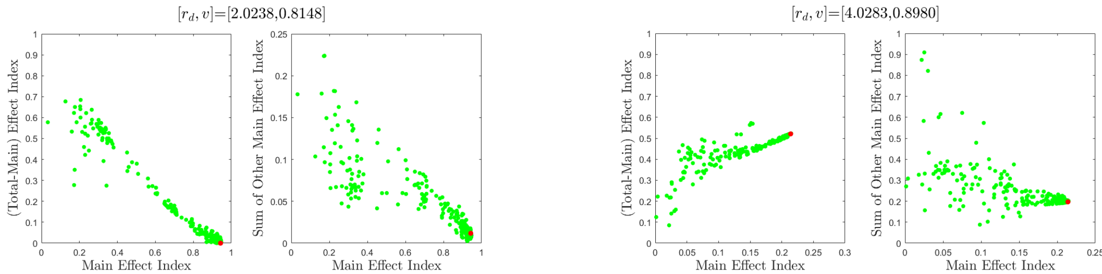

(a) Optimization of cornering stiffness in steady state circular maneuver

(b) Optimization of camber stiffness in steady state circular maneuver

FIGURE 17. Optimization of system parameters in steady state circular maneuver

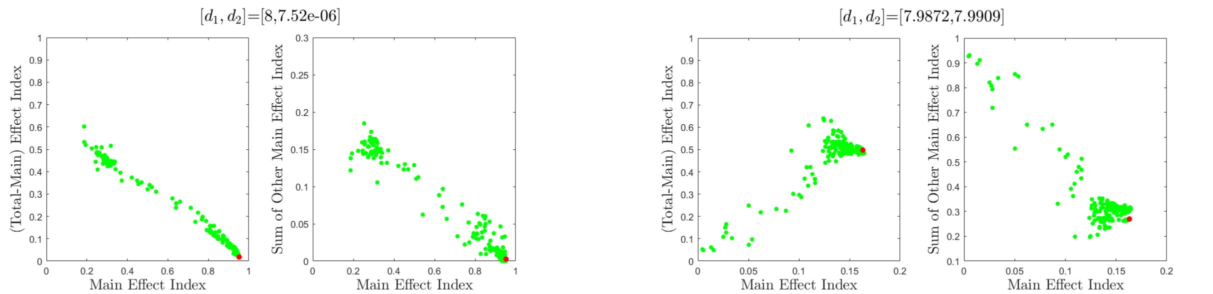

(a) Optimization of cornering stiffness in double lane change maneuver

(b) Optimization of camber stiffness in double lane change maneuver

FIGURE 18. Optimization of system parameters in double lane change maneuver

model-independent method for global sensitivity analysis of model output. *Technometrics*, 41(1):39–56, 1999.

[18] R. Jin, W. Chen, and T. W. Simpson. Comparative studies of metamodelling techniques under multiple modelling criteria. *Structural and Multidisciplinary Optimization*, 23(1):1–13, 2001.

[19] T. J. Santner, B. J. Williams, W. Notz, and B. J. Williams. *The design and analysis of computer experiments*, volume 1. Springer, 2003.

[20] R. Jin. *Enhancements of Metamodeling Techniques in Engineering Design*. PhD thesis, University of Illinois at Chicago, Chicago, IL, 2004.

[21] S. Joe and F. Y. Kuo. Remark on algorithm 659: Implementing sobol's quasirandom sequence generator. *ACM Trans. Math. Softw.*, 29(1):49–57, March 2003.

[22] Y. Huang and K. Chan. A Modified Efficient Global Optimization Algorithm for Maximal Reliability in a Probabilistic Constrained Space. *Journal of Mechanical Design*, 132(6), 05 2010. 061002.

[23] N. A. Cressie. The origins of kriging. *Mathematical Geology*, 22:239–252, 1990.

[24] S. Henry and J. W. Woods. *Probability and Random Processes with Applications to Signal Processing*, volume 4 of *10*. Prentice Hall, The address, 3 edition, 7 2002.

[25] I. M. Sobol M. Sensitivity Estimates for Nonlinear Mathematical Models. *Journal of Mathematical Physics, Analysis, Geometry*, 9(4):435–447, 2013.

[26] W. Chen, R. Jin, and A. Sudjianto. Analytical variance-based global sensitivity analysis in simulation-based design under uncertainty. *Journal of Mechanical Design, Transactions of the ASME*, 127(5):875–886, 2005.

[27] A. Saltelli, M. Ratto, T. Andres, F. Campolongo, J. Cariboni, D. Gatelli, M. Saisana, and S. Tarantola. *Global sensitivity analysis: the primer*. John Wiley & Sons, 2008.

[28] M. J. Sasena. *Flexibility and Efficiency Enhancements for Constrained Global Design Optimization with Kriging Approximations*. PhD thesis, University of Michigan, 2002.

[29] R Rajamani. *Vehicle dynamics and control*. Springer Science & Business Media, 2011.

[30] J. Y. Wong. *Theory of ground vehicles*. John Wiley & Sons, 2008.

[31] A Zandieh. Dynamics of a three_wheel vehicle with tadpole design. Master's thesis, University of Waterloo, 2015.

[32] V. Cossalter. *Motorcycle dynamics*. Lulu. com, 2006.

[33] H. Bellem, T. Schönenberg, J. F. Krems, and M. Schrauf. Objective metrics of comfort: Developing a driving style for highly automated vehicles. *Transportation Research Part F: Traffic Psychology and Behaviour*, 41:45 – 54, 2016.